HUMAN-ROBOT INTERACTION

Virtual elasto-plastic robot compliance to active environments

Michael Panzirsch[1]*, Harsimran Singh[1], Xuwei Wu[1], Maged Iskandar[1], Anne Koepken[1], Rute Luz[2], Nesrine Batti[1], Florian S. Lay[1], Ajithkumar Narayanan Manaparampil[1], Luisa Mayershofer[1], Xiaozhou Luo[1], Robert Burger[1], Samuel Bustamante-Gomez[1], Jörg Butterfass[1], Emiel den Exter[2], Werner Friedl[1], Thomas Gumpert[1], Pedro Pavelski[1], Gabriel Quere[1,3], Florian Schmidt[1], Alin Albu-Schaeffer[1,4], Adrian S. Bauer[1], Daniel Leidner[1,5], Peter Schmaus[1], Annette Hagengruber[1], Thomas Krueger[2], Jörn Vogel[1]†, Neal Y. Lii[1]†

Humans exhibit a particular compliant behavior in interactions with their environment. Facilitated by fast physical reasoning, humans are able to rapidly alter their compliance, enhancing robustness and safety in active environments. Transferring these capabilities to robotics is of utmost importance particularly as major space agencies begin investigating the potential of cooperative robotic teams in space. In this scenario, robots in orbit or on planetary surfaces are meant to support astronauts in exploration, maintenance, and habitat building to reduce costs and risks of space missions. A major challenge for interactive robot teams is establishing the capability to act in and interact with dynamic environments. Analogous to humans, the robot should be not only particularly compliant in case of unexpected collisions with other systems but also able to cooperatively handle objects requiring accurate pose estimation and fast trajectory planning. Here, we show that these challenges can be attenuated through an enhancement of active robot compliance introducing a virtual plastic first-order impedance component. We present how elasto-plastic compliance can be realized via energy-based detection of active environments and how evasive motions can be enabled through adaptive plastic compliance. Two space teleoperation experiments using different robotic assets confirm the potential of the method to enhance robustness in interaction with articulated objects and facilitate robot cooperation. An experiment in a health care facility presents how the same method analogously solidifies robotic interactions in human-robot shared environments by giving the robot a subordinate role.

INTRODUCTION

Elasticity is the fundamental advantage of modern impedance-controlled robots (see Fig. 1A). Such active first-order compliance is mainly realized through virtual spatial springs, minimizing a position deviation of the robot from its reference pose. In telerobotics (*1*, *2*), compliance in interactions with a remote environment is particularly relevant because the operator perceives contact forces with delay. For the Analog-1 space mission led by the European Space Agency (ESA) with the German Aerospace Center (DLR) as partner, a control approach [time-domain passivity control for high delays (TDPA-HD)] has been developed recently (*3*) that increased the compliance of the robot in a contact situation until the operator (see Fig. 1B) on the International Space Station (ISS) was informed about this interaction via force feedback. Still, this enhanced compliance was only established when the contact was initiated by the operator's command (in terms of passivity control, energy flows from the human operator toward the robot; see Fig. 2A). Motivated from this observation, the elasto-plastic robot compliance (EPRC), introduced in this work (Movie 1), aims for enhanced compliant behavior when the contact is established by an active agent in the environment, as for instance by a second robot in a multirobot space scenario (energy flows from the robot toward the human operator; see Fig. 2D). Thereby, the EPRC is able to recognize the source of activity (SoA) that initiated the robot motion and induces a position drift to realize an evasive robot motion in case of contacts that do not result from the robot's motion command. In other words, the SoA can be the robot motion command or an active environment, for instance. In contrast with elasticity control, this EPRC functionality can be described as a plastic impedance component because the robot does not retract to the pose of initial contact. Here, plasticity does not refer to a permanent deformation but a previously undescribed type of virtual compliance implemented in the robot controller.

So far, robotic research has mostly focused on passive environments or collision-avoidance strategies in dynamic environments. In particular, control of mobile robots exposed to natural disturbances, such as wind (*4*, *5*) or waves (*6*), requires strategies to compensate for disturbances of such SoAs. On the contrary, the EPRC, developed for manipulators, does not aim to resist the active environment but intentionally evades the SoA.

A similar plastic-compliant behavior can be observed in human interactions. For example, humans comply in an active environment when closing a door if a second person tries to open the door from the opposite side (see Fig. 2C). Thereby, the human perceives an external SoA and follows the door kinematics as long as they agree with the motion of the active environment. Given that the human does not push back to the initial pose when the second human releases the door, this behavior can be interpreted as a plastic compliance. Plastic compliance can also be observed in the cooperation

[1]German Aerospace Center (DLR), Robotics and Mechatronics Center, Wessling, Germany. [2]European Space Agency (ESA), Noordwijk, Netherlands. [3]Institut Polytechnique de Paris, Palaiseau, France. [4]Technical University Munich, School of Computation, Information and Technology, Garching, Germany. [5]University of Bremen, Institute for Artificial Intelligence, Bremen, Germany.
*Corresponding author. Email: michael.panzirsch@dlr.de
†These authors contributed equally to this work.

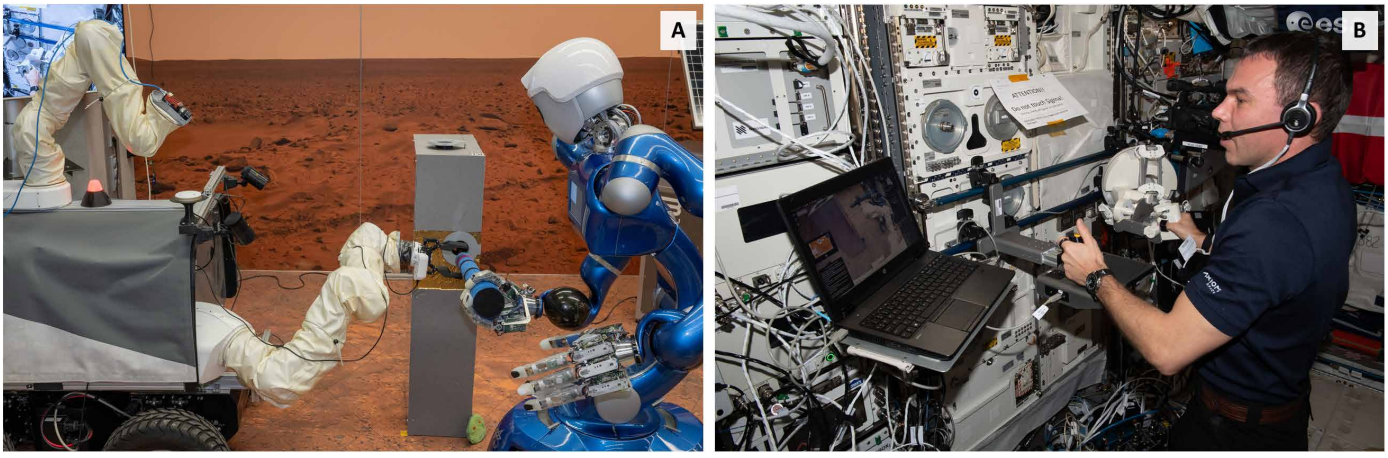

Fig. 1. Setup of the space experiment. (**A**) Team of impedance-controlled robots of DLR's and ESA's Surface Avatar mission. (**B**) Astronaut on the ISS teleoperating the robot team using a haptic interface.

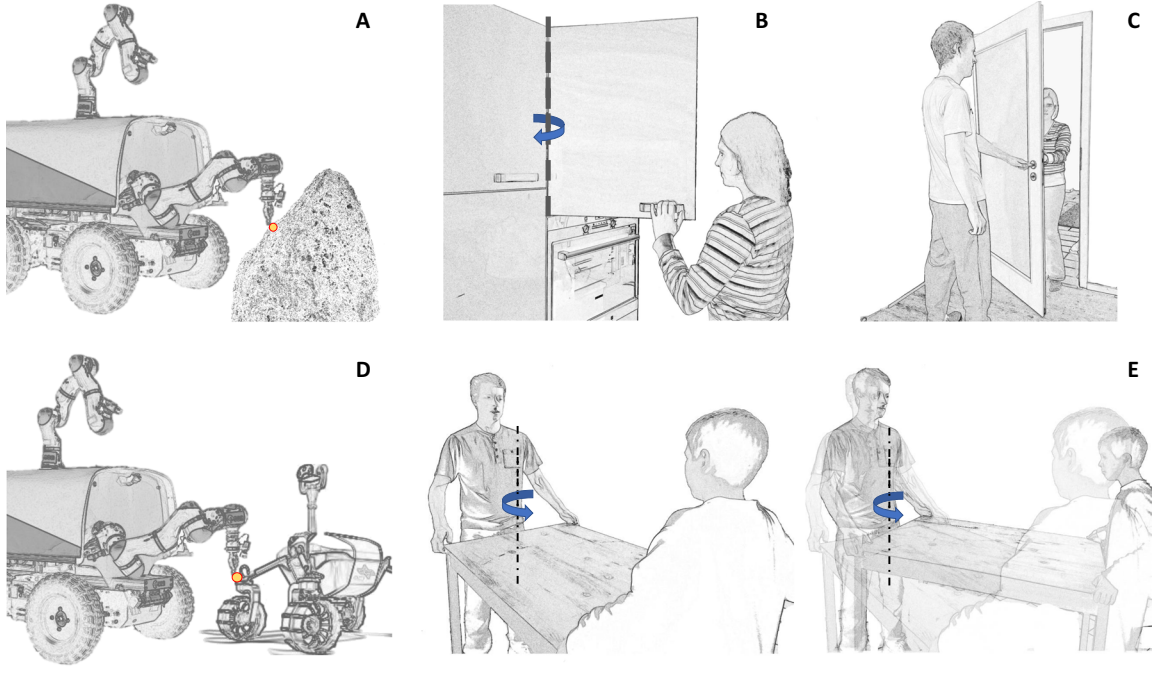

Fig. 2. Robotic and human interactions. (**A**) The motion commanded to a robotic manipulator results in a contact with a passive environment. (**B**) In interactions with articulated objects, humans perceive their kinematics via force sensing and proprioception. (**C**) Two humans interacting with a door from two sides are perceived as active environments by each other. (**D**) A second robot collides with the static left robot. (**E**) Cooperatively handling an object, humans distribute authorities on specific DoFs and behave plastically compliant to the respective higher authority.

between two humans who cooperatively reorientate a table. Thereby, one human has the authority and determines the orientation. The second human supports lifting the weight and complies with the table's motion initiated by the first human by plastically adapting their arm pose (see Fig. 2E). In both cases, the human can completely rely on force perception. No visual information is required here; i.e., the human would be able to behave the same way in the dark without vision.

Such human strategies for leader-follower distribution in cooperative tasks and the role distribution between humans and robots for physical human-robot interaction have already been studied (*7*–*12*) in the literature. Studies on human-human collaboration showed that humans apply leader-follower principles even without verbal communication (*8*) or when humans are not aware of cooperating with another human (*11*). It was found that haptic interaction is crucial for sensory-motor coordination and dyadic coadaptation in collaborative settings (*11*). The roles taken by different agents were observed and distinguished on the basis of interaction forces (*7*, *9*, *13*), reinforcement learning (*7*), or task performance (*8*). In contrast, here, we consider the power flow for role distribution. Furthermore, in the proposed method, the roles can switch in a continuous manner.

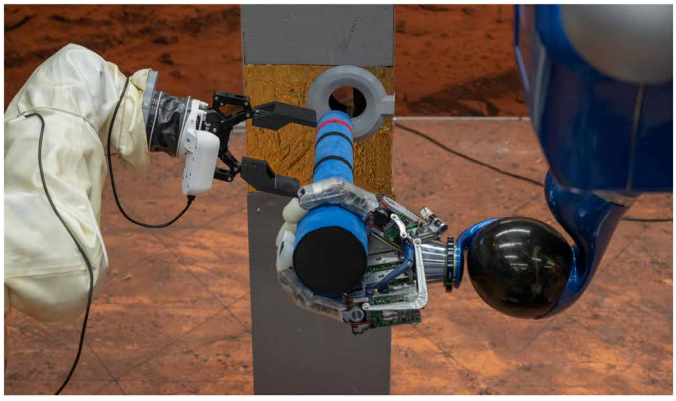

Movie 1. Overview of the elasto-plastic robot compliance method.

The proposed EPRC method realizes plastic reactions adaptive to the SoA in robotics, mimicking leader-follower strategies observable in human interactions within active environments. Hereby, the virtual plastic compliance has a persistent behavior, resulting in a permanent pose adaptation (position drift). Notably, no force-torque sensor at the end effector, disturbance observer, or visual sensing is required to achieve this behavior in EPRC control. Instead, the standard implementation of the EPRC solely requires the robot velocity and the wrench computed by the impedance controller. The EPRC is of particular relevance in delayed teleoperation because it acts as a local support on the robot side. Note that the TDPA-HD (which inspired the development of EPRC) was applied throughout this work to ensure stability despite delayed communication. The EPRC itself is integrated into the impedance controller such that it can be combined with a large variety of control approaches. This work highlights a variety of benefits of this SoA-based plastic compliance, ranging from an increase in the robustness of robot cooperation and handling of articulated objects to applications in human-robot shared environments.

Robot compliance

The necessity for compliant behavior was evident from the early beginnings of robotics control (*14*, *15*). To achieve this relation between interaction force and robot motion, admittance (*14*, *16*) and impedance control (*15*, *17*) were developed. In contrast with admittance control that can only be realized with force-torque sensing, impedance control can also be achieved implicitly without dedicated force-torque sensors at the end effector. Later research focused on human-like impedance behavior (*18*, *19*) and even biomimetic control adapting force and impedance by minimizing the metabolic cost (*20*). In recent years, impedance control has received increasing popularity because of the emerging availability of comparably low-cost robots equipped with joint torque sensors enabling active compliance (*21*–*23*). One category for the next generation of robot hardware will be based on so-called passive compliance that is achieved through elastic design on the actuator level (*24*, *25*). Still, elastic joints are not necessarily safer with regard to metrics such as the head injury criterion and frontal or abdominal impact force (*26*). It must be considered that the system stiffness still depends on the applied control strategy and that the system can store potentially harmful energy. Hence, although adaptive robot compliance (*27*, *28*) is highly beneficial, the logic of compliance adaptation is even more crucial. Conventionally, in the case of active or passive compliance, the external forces can be estimated robustly through momentum-based observers (*29*, *30*). That is practically beneficial to provide the robotic system with essential safety features such as collision reaction strategies (*31*, *32*).

The main aspects of the proposed EPRC are its plasticity as a previously undescribed level of active robot compliance and the sensitivity to the SoA ensuring that this compliance is triggered in the correct instant. This intelligent adaptivity renders the method particularly beneficial, as will be explained later.

Robots in human-robot shared environments

Recent ambitions aim to introduce service robots with manipulators in health care assistance settings (*33*–*35*) or comparable human-robot shared environments (*36*). There, robots must be particularly compliant when humans are detected in the environment. Current safety regulations for robots in coexistence or cooperation scenarios (*37*, *38*) were developed mainly for industrial settings. Norms and standards that need to be accounted for span from technical specifications for collaborative robots [International Organization for Standardization (ISO) 15066/TS] and general norms related to risk (ISO 14971) and quality management (ISO 13485) to safety requirements for personal care robots (ISO 13482).

The primary safety requirement is the reliable detection of humans on the basis of visual (*39*), force (*40*), disturbance, or other collision sensors. Nevertheless, health care settings are highly dynamic environments with complex object characteristics, such as the intrinsic damping of a door, that can hardly be modeled with sufficient accuracy. Therefore, these norms and standards would, for instance, not allow a robot to open a nontransparent door using current control solutions because a human acting on the door from the other side cannot be reliably detected.

The proposed EPRC pursues a previously undescribed path by observing the SoA in the environment, evading contact in case of an active environment, and thus putting the robot into a subordinate role. Thereby, the EPRC maintains the full capabilities of the robot in terms of applicable interaction forces. In contrast with the EPRC, comparable existing methods (*40*) require highly accurate environment modeling or limitation of control forces to a safe threshold, critically reducing the robot's capabilities.

Contributions

In summary, the core contribution of this work is the concept of virtual elasto-plastic robot compliance as a previously undescribed class of active robot compliance adaptive to the SoA in the robot environment. This includes a requirement definition for two types of SoA, as well as the design and the implementation of the EPRC functionality. In addition, we validate the proposed method in complex applications involving space and health care scenarios. The resulting previously undescribed category of robot compliance promises to solidify interactions of robots in and with active environments in terms of robustness in task execution and safety.

The fundamental functionality of the EPRC is a plastic reaction to energy inputs from the environment. This energy input or SoA can result from a real active environment (SoA type 1) as a human, another robot, or a natural disturbance such as wind or waves. Alternatively, the energy triggering the EPRC can also be reflected

by an articulated object, such as a door, that the robot interacts with. Thereby, the robot itself may introduce energy in one DoF (degree of freedom) that is partially reflected by the door kinematics in another DoF as visualized in Fig. 2B. There, a human pulls a cabinet door open toward their body, perceiving a force and motion (energy input) in a perpendicular direction. A human can comply with this energy input to perfectly follow the door handle trajectory. This interaction with articulated objects will be referred to as a pseudoactive interaction (SoA type 2) in the remainder of this manuscript.

In the case of an active environment (SoA type 1), the EPRC brings various benefits to robot control. In accordance with the aforementioned norms and standards, the EPRC puts the robot into a subordinate role while not requiring conservative force limitation or modeling of environments. We performed a space experiment presenting how the EPRC eases the cooperation of two robots in an insertion task if one robot complies with the motion of the other in a plastic manner. With this scenario, the EPRC enabled a six-DoF cooperative space experiment involving teleoperation from the ISS with a round-trip communication delay above 800 ms. Furthermore, we present an experiment in an elderly care facility in which a human tried to open a door that was grasped by a robot on the opposite side. During this procedure, the EPRC initiated an evasive motion of 46 cm, whereas, with the same force, the human could have opened the door by only 2.3 cm without the EPRC. In addition, we present the benefits of the EPRC in interaction with articulated objects (SoA type 2): In the space experiment with delayed perception of the teleoperator, the EPRC compensated for 54.7% of the motion required to follow a trajectory while handling an object with circular kinematics. Further laboratory experiments confirm that with optimal parametrization, this compensation can be increased above 80%, underlining the vast potential of the proposed method.

RESULTS

Desired behavior and design goals

The desired capabilities of the EPRC are discussed in the following section with the help of the scheme in Fig. 3. To provide the expected functionality, the EPRC has to be able to infer whether a robot motion resulted from a robot control command or an active environment. In the first case, the motion command leads to a deflection of the coupling spring (the most essential component of the impedance controller) that generates a force aiming to minimize a deviation of the robot and reference pose. A purely elastic behavior is visualized in the left column in Fig. 3. In the scenario of the middle column, the robot pose is varied by an active environment. The plastic compliance is realized by updating the reference pose with the respective robot pose change resulting from the interaction with an active environment. Therefore, the reference pose deviates from the commanded pose after plastic reaction. Given that the coupling spring is not deflected, the robot is not pushed to the initial pose. When the force applied by the active environment overcomes the force of an elastic spring component that has already been deflected, the robot starts moving in the direction of the applied force, as visualized in a combination of elasto-plastic compliance in the right column of Fig. 3. Then, the EPRC recognizes the active environment and accounts for the position change as a plastic motion, preventing an additional deflection of the coupling spring.

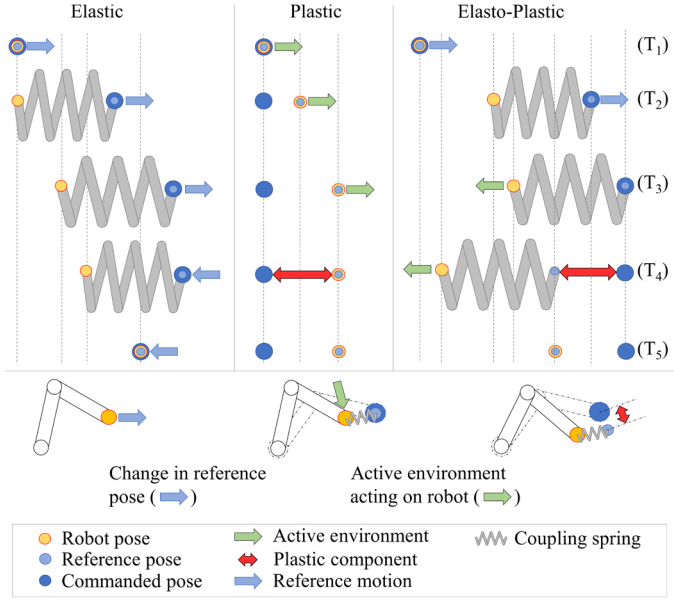

Fig. 3. Human-like elasto-plastic behavior. A virtual elastic spring pushes the robot pose to the commanded pose (≡ reference pose). In interactions with active environments, robots can react plastically, similar to humans. This can be achieved by updating the reference pose (≠ commanded pose) with the variation of the robot pose. This elastic and plastic behavior can coexist in an elasto-plastic controller.

The door scenario outlined in the introduction effectively illustrates the functionality of the EPRC. Let us imagine that the robot is pulling with an arbitrary force on a door to open it. This corresponds to situation (T_2) in Fig. 3. Thereby, the robot motion reference deflects the virtual coupling spring and generates a force F^c acting on the door. Next, a human (active environment) pulls from the opposite side to close the door (T_3). As soon as the pulling force of the human is higher than the robot control force F^c, the active environment is recognized, and a plastic reaction is triggered by the EPRC. Thus, the robot follows the human's motion (T_4) while the spring deflection is maintained. Consequently, the EPRC assigns the robot a subordinate role, enabling it to comply with the human motion without relying on visual input, external force sensing, or environmental knowledge.

In addition to this functionality, the EPRC needed to meet further requirements not addressed by comparable approaches. These include allowing the robot to apply unrestricted force and eliminating the need for environment modeling, disturbance observers, or force-torque sensors at the end effector.

Detecting the SoA

The fundamental principle of the EPRC control action is to determine whether the control command or an active environment caused a robot motion by analyzing the SoA. This requires the observation of the energy flow in the system. For that reason, the one-DoF network representation depicted in Fig. 4 is deduced from the signal flow diagram of the coupling controller, which generally consists of an elastic component storing potential energy with the stiffness K and the dissipative damping element B. It should be noted that the damping B influences the optimal parametrization of the EPRC but is neglected here for the sake of simplicity. The

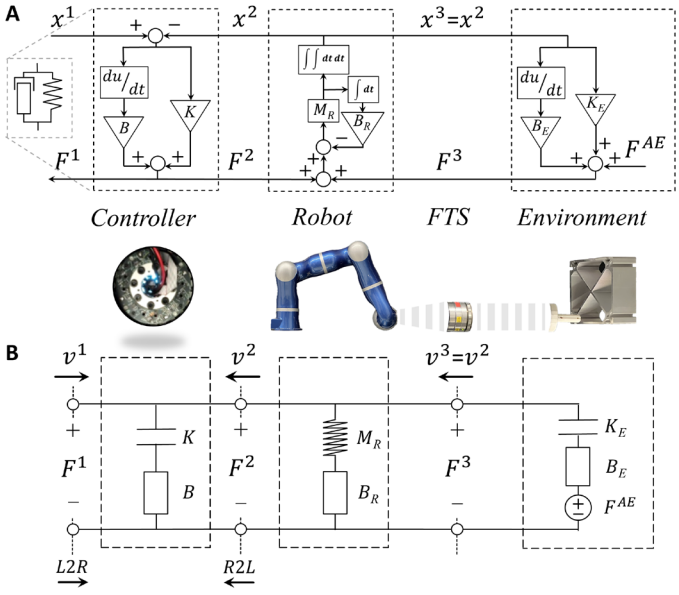

Fig. 4. Modeling the control loop. (**A**) The coupling controller compares the reference motion x^1 with the robot pose x^2 and generates a force F^2 for the sake of position convergence. A potential force-torque sensor (FTS) measures the direct interaction force F^3 between robot and environment. (**B**) Through the corresponding network representation, the system energy flow can be observed. The energy exchange with the robot's environment can be measured via v^2 and F^2 (or v^2 and F^3 more accurately) on the robot side.

coupling controller compares the reference pose x^1 and the robot pose x^2 and generates a force F^2 that pushes the robot to the reference pose. The network representation provides power ports on the basis of flow (velocity v) and effort variables (force F). These variables represent a power-conjugate pair such that the power and energy flow at the respective port can be determined via multiplication and integration: The power P_m^i in a translational DoF $m \in \{1, 2, 3\}$ is calculated via the correlated signal robot velocity v^i and wrench F^i at port i: $P_m^i(t) = v_m^i(t)F_m^i(t)$. Because the rotational DoFs $m \in \{4, 5, 6\}$ are coupled and need to be considered conjointly, the overall rotational power sum P_{rot}^i was used in the EPRC in the rotations: $P_{\text{rot}}^i(t) = \sum_{m=4}^{6} v_m^i(t)F_m^i(t)$. Through the sign of the power, the energy flow direction can be analyzed. An active environment can be observed if a power $P_{\text{R2L}}^{\text{env}}$ flows at the robot side port $[v^2, F^2]$ in a right-to-left direction (R2L). The EPRC variable $\varepsilon(t)$ indicates an active environment if the power $P_{\text{R2L}}^{\text{env}}$ is larger than the threshold P_{thr} and the computed force F^{c} exceeds the threshold F_{thr}

$$\varepsilon(t) = \begin{cases} 1 & \text{, if } P_{\text{R2L}}^{\text{env}}(t) > P_{\text{thr}} \,\&\&\, |F^{\text{c}}(t)| > F_{\text{thr}} \\ 0 & \text{, else} \end{cases}$$

Note that if a force-torque sensor is available on the robot end effector, the active environment can be determined more accurately via the power-conjugate pair of robot velocity v^2 and the measured force F^{m}. Thus, the effects of robot dynamics on the EPRC parametrization can be reduced at a potentially higher cost. Here, we restricted the EPRC implementation to computed wrenches; i.e., no measured wrench was considered. Alternatively to the power-based formulation, an energy-based version of the EPRC is presented in the Supplementary Materials ("Energy-Based Implementation of EPRC" section) including the discussion of benefits of both methods.

The control action

In a standard elastic coupling, the robot motion reference $x^{\text{R}'}$ can be deduced directly from the initial robot pose $x^{\text{R}}(t_0)$ via integration of the commanded velocity $v^{\text{R}^*} = v^1$. When EPRC is triggered by an active environment ($\varepsilon = 1$), the robot motion $v^{\text{R}} = v^2$ is considered in the integral element in addition

$$x^{\text{R}'}(t) = x^{\text{R}}(t_0) + T_{\text{s}} \sum_{\tau=t_0}^{t} \left(v^{\text{R}^*}(\tau) + \varepsilon(\tau) v^{\text{R}}(\tau) \right) \tag{1}$$

to the sampling time T_{s}. Thus, the robot complies with an active environment because the EPRC prevents a deflection of the spring. The multi-DoF implementation of the EPRC, including the more complex distribution of elastic and plastic motions in the rotational DoF, as well as the passivity discussion, is presented in the Supplementary Materials ("Implementation of Power-Based EPRC" section).

Abstract laboratory experiments

The initial analysis of the approach presented in the following was performed with a DLR lightweight robot (LWR) teleoperated via the haptic input device lambda.7. The laboratory experiments served as validation of the EPRC principle and as the test of robustness during wall contacts and free motion phases.

During the experiment shown in Fig. 5A, the robotic manipulator ${}^{\text{W}}\mathbf{H}_{\text{R}}$ was moved by an active environment (human arm), whereas the input device ${}^{\text{W}}\mathbf{H}_{\text{R}^*}$ was static. The power threshold was set to $P_{\text{thr}} = 0.1$ J/s and the force threshold to $F_{\text{thr}} = 0.4$ N. It could be observed that the robot complied with the active environment (robot reference pose ${}^{\text{W}}\mathbf{H}_{\text{R}'}$ follows ${}^{\text{W}}\mathbf{H}_{\text{R}}$), whereas the interaction force with the active environment was below 4 N.

The second experiment displayed in Fig. 5B focused on contacts of the manipulator with a stiff environment, which resulted from a motion command of the input device. As expected, no active environment was recognized ($P_{\text{R2L}}^{\text{env}} < P_{\text{thr}}$) besides two short instances. A slight increase in the power threshold or an additional criterion considering the robot velocity would help to avoid this erroneous detection. Still, the plastic reaction was negligible because of the very low robot velocity during contact such that an adaptation of the threshold was unnecessary. It is important to note that the operator could apply arbitrary forces against the environment because the EPRC does not require conservative force limitation.

The third abstract experiment presented in Fig. 5C served as a robustness test during free motion with high acceleration and deceleration to investigate the influence of the robot dynamics. Again, ε remained zero as desired because the deadband of $P_{\text{R2L}}^{\text{env}}$ was not reached.

In contrast with the first experiment confirming the functionality of the EPRC control concept, the latter two experiments underlined the robustness of the approach. Further experiments in the Supplementary Materials ("Supplementary Methods" section) provide more insights into the EPRC performance during soft wall contacts and the benefits of an energy-based detection of the SoA among others.

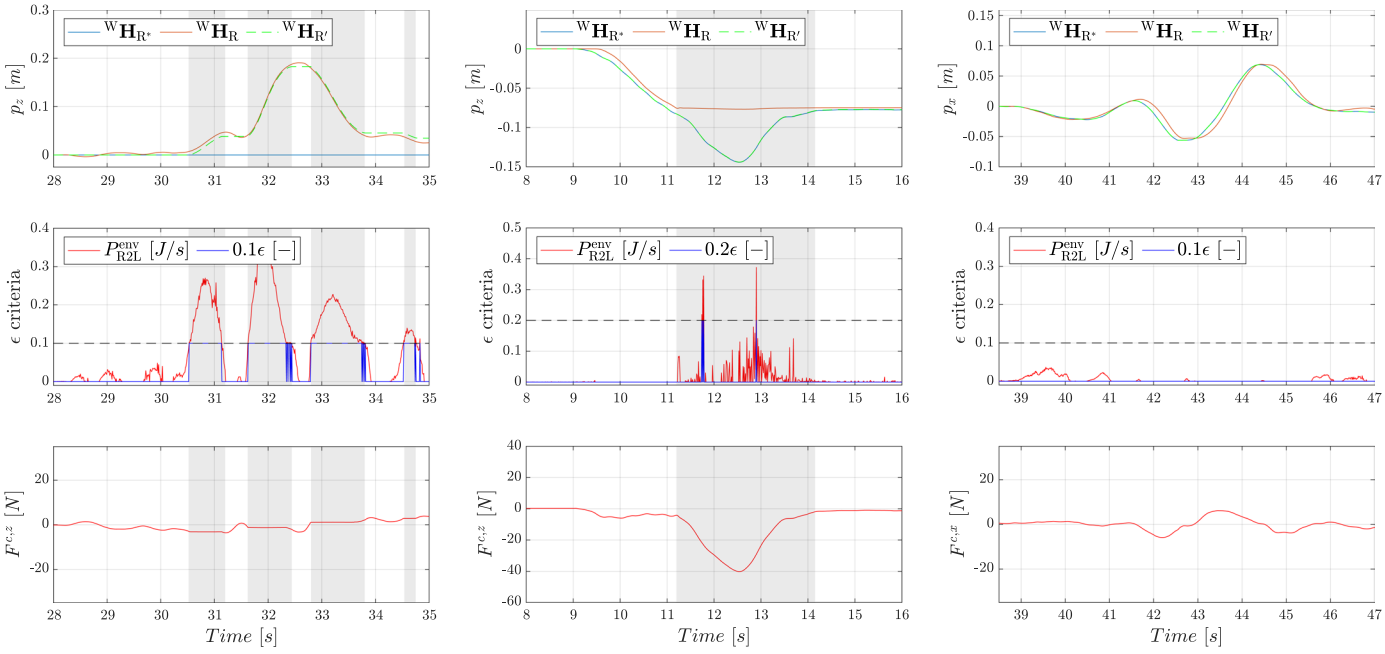

A SoA Type 1: Interaction with active environment.

B Hard contact w/o active environment.

C Fast free motion w/o active environment.

Fig. 5. Abstract laboratory evaluation. The dashed lines indicate the power threshold. (**A**) SoA type 1: interaction with active environment. An active environment (marked with shaded background) moves the robot. The EPRC recognizes the active environment and adapts the robot reference pose $^{W}\mathbf{H}_{R'}$ corresponding to the robot motion $^{W}\mathbf{H}_{R}$. (**B**) Hard contact without active environment. The robot contacts a stiff wall (marked with shaded background). Although the power threshold is slightly crossed in some instances, the plastic reaction of the EPRC is negligible as desired. (**C**) Fast free motion without active environment. Despite slight position overshoots of the robot during fast robot motion, no active environment is recognized.

Evaluation in realistic scenarios

The EPRC promises benefits in various applications. Evasive plastic motions to active environments (SoA type 1) can increase safety in human-robot shared environments and ease robot collaboration. In the same way, errors in odometry in mobile systems can be compensated for and bimanual interaction can be robustified in case of non-optimal grasp observation through the EPRC. Furthermore, plastic reactions during interactions with articulated objects (SoA type 2) promise to increase the robustness in task execution. This was verified in a space experiment, in which the operator had reduced perception of the object kinematics because of a delay in the visual and the force-feedback channel and mono instead of stereo visual feedback. SoA type 1 was examined in the initial six-DoF space experiment with a collaborative robot team and in a human-robot interaction scenario featuring a health care assistance robot in an elderly care facility. The latter experiment was performed by an expert teleoperator, whereas the astronaut in the first experiment was a novice in teleoperation and was working with EPRC support for the first time.

The combination of elastic and plastic behavior of the EPRC is a unique feature in compliance control. To highlight its advantages, we investigated three metrics: first, the percentage of commanded motion, $p_{\%} = (p_{com} - p_{ref})/p_{com}$, that became unnecessary for following a trajectory along an object kinematic when the EPRC compensation was active. This metric indicates by how much the operator's effort was reduced. Second, a metric for the deflection of the spring $\Delta p = F^{c}_{max} / K^{t}$ was considered, which indicates how much the robot would have complied with an active environment without EPRC control. Thereby, F^{c}_{max} represents the maximal force and K^{t} represents the stiffness of the coupling controller. Third, the ratio $R_{\%}$ between the potential elastic reaction Δp versus the EPRC drift $p_{com} - p_{ref}$ further emphasizes the advantage of elasto-plastic behavior over pure elastic compliance: $R_{\%} = \Delta p/(p_{com} - p_{ref})$.

Figure 6 presents the trajectories of the commanded pose $^{W}\mathbf{H}_{R^*}$, the reference pose $^{W}\mathbf{H}_{R'}$ after adaptation through the EPRC, and the robot pose $^{W}\mathbf{H}_{R}$ resulting from the following experiments. More detailed signal plots on the respective experiments are presented and discussed thoroughly in the Supplementary Materials ("Supplementary Discussion" section).

SoA type 1: Collaboration of a rover-based manipulator and a humanoid robot in the Surface Avatar ISS-Earth telerobotic mission

Our approach was implemented in the Surface Avatar ISS-Earth Telerobotic mission led by DLR with ESA as partner. This was the first series of teleoperation experiments with a surface robotic team teleoperated from space (*41*, *42*). Figure 6A shows the trajectories of two robots during a collaborative pipe insertion task. The left-hand robotic manipulator of the ESA Interact Rover (IR) was controlled by an astronaut on the ISS at a round-trip delay (RTD) of ~850 ms via a sigma.7 haptic input device providing force feedback to display the interaction wrench measured by a force-torque sensor at the robot's end effector. The TDPA-HD ensured stability despite delayed communication. The two robots cooperatively grasped a pipe that had to be inserted into a plug in the wall. The humanoid robot DLR

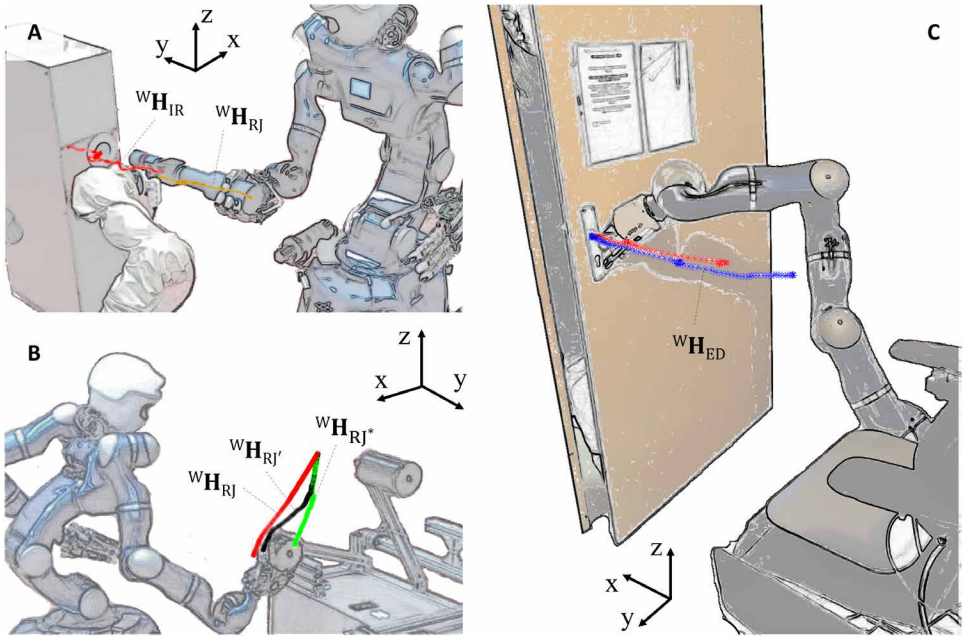

Fig. 6. Active and pseudoactive interactions in realistic scenarios. (**A**) A six-DoF robot collaboration (SoA type 1) controlled from the ISS. (**B**) An interaction with an articulated object (SoA type 2) of a robot controlled from the ISS. (**C**) An evasive motion during human-robot interaction (SoA type 1).

Rollin' Justin (RJ) on the right was in Cartesian impedance control and autonomous mode, although the robot could also be teleoperated while maintaining the capability to react plastically whenever the EPRC control was triggered. In this scenario, the humanoid robot could autonomously set the correct orientation but needed support in inserting the pipe. The EPRC was enabled only in the translations such that the humanoid robot obeyed the translational motion of the second robot teleoperated from the ISS, acting as an active environment on the humanoid robot. This cooperative task design not only allowed handling higher loads but also enabled the manipulator of the rover to release and regrasp objects, for instance, in case the robot arm occluded the insertion area.

The focus of this experiment was on investigating the effects of delay and microgravity. The RTD of about 850 ms led to deficits in perception of the remote robot environment because the visual and force feedback did not correspond exactly to the remote situation. Furthermore, the precision was reduced given that only mono visual feedback was provided because of bandwidth limitations. Apart from these natural circumstances, the TDPA-HD controller, which ensures stability despite communication delays, affected position tracking and force-feedback quality, further diminishing perception. The reader is referred to (*3*) for more details on TDPA-HD. In addition to these artifacts, the TDPA-HD potentially attenuates the power flow to the environment, which potentially reduces the sensitivity of activity detection needed to trigger EPRC. Furthermore, astronauts suffer from disturbed proprioception (*43*, *44*) especially in the early phase of adaptation to microgravity. Given that the astronaut had only been on the ISS for 6 days at the time of the experiment, they potentially had difficulties in accurately positioning their arms and in perceiving kinesthetic interaction forces with the haptic device, which may have further limited their task performance. These challenges motivated the evaluation of the EPRC under delay and in microgravity.

Despite these circumstances, the untrained astronaut was able to move the IR firmly enough to overcome the power threshold $P_{\text{thr}}^{\text{RJ}} = 0.01$ J/s and force threshold $F_{\text{thr}}^{\text{RJ}} = 0.05$ N of the EPRC to initiate a plastic reaction of the humanoid robot. It could be analyzed from the trajectories in Fig. 6A that the astronaut first commanded the robot $^{W}\mathbf{H}_{IR}$ into contact with the front of the board, then moved the robot slightly in the positive x direction, and finally managed to insert the pipe. During this insertion procedure, the arm of the humanoid robot had to move ~33 cm in EPRC control. Thereby, the astronaut applied a maximum force of 7.0 N. The astronaut successfully performed the plug insertion three times, each with different clearances (1.0, 0.6, and 0.4 cm) between the plug and the pipe (with a diameter of 6.5 cm).

Further plots and a picture sequence are presented in the Supplementary Materials ("SoA Type 1 Space Scenario" section). From those, it can be analyzed that the humanoid robot's behavior was highly reactive and compliant with the motion of the rover manipulator despite delay artifacts.

SoA type 2: Interactions of a humanoid robot teleoperated from ISS with an articulated object

In the second space experiment, the astronaut aboard the ISS controlled the humanoid robot RJ. The TDPA-HD was also implemented on the humanoid robot, but because of the absence of a force-torque sensor at the end effector, the external wrench estimated by a disturbance observer was applied as force feedback. The task was to move a lever, an articulated object (pseudoactive interaction, SoA type 2) with circular kinematics, around an axis up and down (see Fig. 6B). Through this axis, energy could be transferred from one DoF to another, triggering an activation of the EPRC.

In addition to the evaluation of delay and microgravity effects in the previous experiment, the focus of this experiment was on the performance of the EPRC during transitions between plastic and elastic behavior. In contrast with the space experiment on SoA type 1, the EPRC-controlled robot was teleoperated such that all Cartesian DoFs could be operated by the astronaut but behave plastically at the same time whenever the EPRC was triggered. Thereby, the EPRC did not require switching to a different control state but enabled continuous transitions. Regarding the delay, the EPRC acting locally at the robot side revealed particular advantages during control of articulated objects (SoA type 2). In teleoperation, the force feedback supported the operator substantially in following the kinematics of a handled object. However, the higher the delay, the more the perception and the force-feedback quality suffered, rendering kinematically restricted tasks more difficult. Because the EPRC corrected the robot command locally at the robot side, the effects of delay were reduced such that the operator needed to correct less. In

contrast, the kinematic support via force feedback would have been effective only after one RTD when the respective pose correction, initiated by the operator as a reaction to the force feedback, was commanded to the robot.

Figure 6B shows the trajectory of the robot ${}^{W}\mathbf{H}_{RJ}$, the motion ${}^{W}\mathbf{H}_{RJ^*}$ commanded via the input device, and the motion reference ${}^{W}\mathbf{H}_{RJ'}$ generated by the EPRC. In the presented phase of the experiment, the operator was asked to command a straight motion via the input device to move the lever downward (z direction) starting from a position corresponding to the lever depicted on the right. The trajectory ${}^{W}\mathbf{H}_{RJ}$ depicts the motion path of the end effector. Given that the hand was slightly rotating because of rotational elasticity, the path was not perfectly circular. Furthermore, the input device was not moved perfectly straight downward. This may be due to not only the reduced proprioception in the early phase of adaptation to microgravity but also the force feedback supporting the operator in following the robot's trajectory.

The EPRC was enabled in translation and parametrized with a force threshold of $F_{thr}^{RJ} = 0.4$ N and a power threshold of $P_{thr}^{RJ} = 0.2$ J/s. Despite the reduced proprioception, the communication delay, and the limited experience of the astronaut, the EPRC reduced the required motion in the x direction by $p_{\%} = 59\%$. Detailed plots and a picture sequence of the experiment are presented in the Supplementary Materials ("SoA Type 2 Space Scenario" section).

The whole procedure (up and down motion of the lever) was performed with and without the EPRC. Although the astronaut was asked to move the input device only up and down with the EPRC, resulting in high control forces when compared with perfect matching of the kinematics, the mean force $mean(F^c)$ applied by the robot varied only about 19.2% [with EPRC: $mean(F^c) = 25.8$ N, without EPRC: $mean(F^c) = 21$ N]. Given that the operator did not try to match the lever trajectory when using the EPRC, higher forces were expected in that case.

The comparably high value of P_{thr}^{RJ} was chosen out of safety considerations because of unexpected artifacts that potentially result from a space setup and an untrained operator. Still, the initial large offset between ${}^{W}\mathbf{H}_{RJ^*}$ and ${}^{W}\mathbf{H}_{RJ}$ is an artifact of the high power threshold that was not overcome until one-third of the downward motion. More detailed plots on this experiment and a laboratory experiment with another articulated object are presented in the Supplementary Materials ("SoA Type 2 Space Scenario" and "Experiments with Power-Based EPRC" sections, respectively).

SoA type 1: Human-robot interaction in an elderly care facility

In contrast with the preceding experiments that were performed in a multirobot space scenario, the final experiment took place in an elderly care facility, allowing for the evaluation of the EPRC performance in a human-robot shared environment (see Figs. 6C and 7). The approach was implemented on the wheelchair-based manipulator of the health care assistant robot DLR EDAN (Electromyography-controlled Daily AssistaNt). In this scenario, while trying to open a door, a human (representing an active environment, SoA type 1) unexpectedly interacted with an occluded robot on the other side of the door. Note that the EPRC can also support closing the door as an articulated object (pseudoactive interaction, SoA type 2), but the following analysis focused on the interaction with the human (SoA type 1).

The focus of this evaluation was on the influence of the type of SoA and the EPRC performance on a robot while being teleoperated. Here, the energy triggering the EPRC was transferred from the human to the robot directly via the door. In contrast with the SoA type 1 space scenario, the energy was transferred through neither a communication channel nor a second robot.

The EPRC was enabled in all six Cartesian DoFs ($P_{thr}^{ED,t} = 0.01$ J/s, $P_{thr}^{ED,r} = 0.1$ J/s, $F_{thr}^{ED,t} = 0$ N, $F_{thr}^{ED,t} = 0$). Figure 6C depicts the trajectory of the robot ${}^{W}\mathbf{H}_{ED}$ in the elderly care facility. Note that the manipulator of the wheelchair-based robot DLR EDAN was teleoperated from the same facility via a sigma.7 input device, resulting in an RTD below 100 ms such that the EPRC performance was not expected to be impaired by the communication delay. Nevertheless, the TDPA-HD was implemented. Because of the absence of a force-torque sensor at the end effector, the external wrench estimated by a disturbance observer was applied in TDPA-HD. The lower trajectory marks the robot's path while initially trying to close the door. When the door was almost closed, a human tried to enter the room. Because the robot was in EPRC control, the robot was able to recognize the active environment and evaded the door's motion as depicted by the upper trajectory in Fig. 6C. Thereby, no visual detection of the human or path planning of the robot was required. Without need for reset or state changes, the teleoperator was directly able to apply forces after the human had entered the room such that they could subsequently close the door.

During the evasive motion, the manipulator of EDAN was moved plastically about 40.85 cm (see experimental data in Fig. 7G). In the course of this procedure, the robot resisted with a maximum force of $F^c = 14$ N against the human motion. In case of a purely elastic controller ($K = 600$ N/m), this force would have enabled opening the door by only $\Delta p = 2.3$ cm ($R_{\%} = 5.63\%$) such that the human would not have been able to enter the room. To analyze more detailed plots, the reader is referred to the Supplementary Materials ("SoA Type 1 Healthcare Scenario" section).

DISCUSSION

This work introduced the principle of the EPRC for cooperation and coexistence scenarios with validation in a space and a health care assistance context. Thereby, the straightforward integration of the EPRC in three different robotic setups underlined the modularity and high versatility of the controller. Overall, the experiments confirmed that the proposed EPRC is sensitive to the SoA and fulfills the respective design goals deduced from human plastic behavior in interactions with active environments and articulated objects. The evaluation during a space mission and in the elderly care facility confirmed a high technology-readiness level of the EPRC and its relevance in a variety of control challenges.

Laboratory evaluation

The abstract laboratory experiments confirmed the capability of the EPRC to trigger plastic reactions without losses in robot performance. Furthermore, the robustness of SoA detection was verified during contacts with passive environments and considering motion commands of high acceleration and deceleration. The power-based EPRC version, as implemented for the space and health care scenarios, was confirmed to be sufficient in all scenarios investigated in this work. Additional experiments in the Supplementary Materials ("Experiments with Energy-Based EPRC" section) highlighted that an energy-based

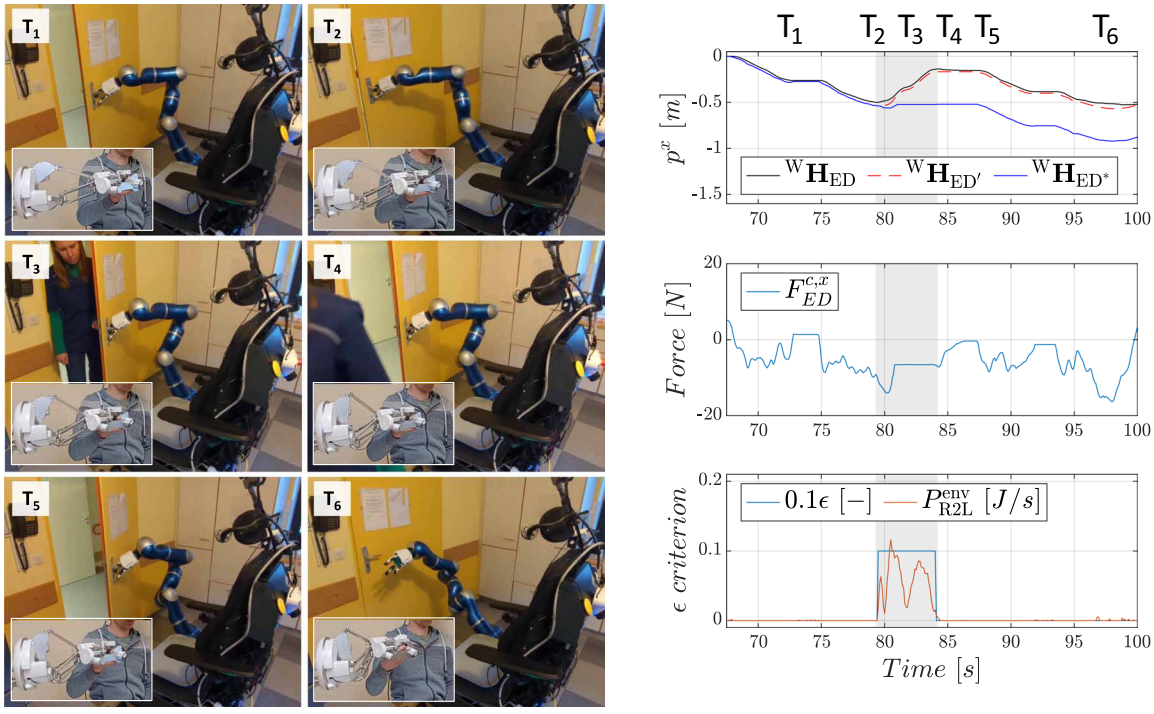

A Picture sequence. **B** Experimental Data.

Fig. 7. SoA type 1 health care experiment. (**A**) Picture sequence. First, the teleoperator tried to close the door moving ~50 cm (T_1-T_2, t = [68 s, 79 s]). Then, a human entered the room such that the robot recognized an active environment and evaded the human plastically for about 40 cm (T_3-T_4, t = [79 s, 84 s]). As soon as the environment behaved passive, the teleoperator was able to control the robot in all DoFs and to close the door (T_5-T_6, t = [84 s, 100 s]). (**B**) Experimental data. The robot reference pose $^{W}\mathbf{H}_{ED'}$ followed the robot pose $^{W}\mathbf{H}_{ED}$ when an active environment was recognized ($\varepsilon = 1$).

EPRC implementation has comparable performance. Because this version requires energy resets, which make the control less continuous, this work focuses on the power-based EPRC. Nevertheless, the energy-based version promises to increase robustness in the gravity direction and thus might prove advantageous when carrying heavy objects in future work.

SoA type 1 evaluation in space and health care application

With the more realistic EPRC application in a space mission involving an astronaut with limited experience in robot control of this style and the application in a health care facility with human-robot interaction, the EPRC robustness was successfully validated. In the cooperative space experiment, the EPRC showed the expected level of performance, although the force initiating the plastic reaction of the humanoid robot was applied indirectly via a second impedance-controlled robot. Although passivity control attenuated the power transmitted from the operator aboard the ISS, the robustness against immense delay could be confirmed. The insertion task, one of the most challenging types of tasks in robot control, was successfully performed three times with varying clearances between the pipe and hole (1, 0.6, and 0.4 cm) each time. Furthermore, it should be noted that the astronauts repeatedly mentioned that the collaborative, EPRC-enabled robot provided immense support in task execution. The EPRC enabled the astronaut to release and regrasp the pipe during the last of the three insertion trials when the teleoperated arm occluded the insertion point. These capabilities and the astronaut's feedback highlight the potential of the EPRC support in more complex robotic space applications in the future. Additionally, the metrics on spring deflection resulting in a case without the EPRC $\Delta p = 1.4$ cm and the ratio $R_{\%} = 4.7\%$ comparing Δp and the elasto-plastic compliance $p_{\text{com}} - p_{\text{ref}}$ confirmed the advantages of the plasticity control method in the cooperative space experiment. Regarding the translational stiffness $K^{t} = 500$ N/m of the RJ manipulator, applying a force of maximally $F^{c} = 7.0$ N, the robot would have moved only 1.4 cm in case of impedance control without a plastic component. In contrast, the EPRC induced a plastic motion of 33 cm, an increase of more than 2250%. It is notable that if DLR RJ was teleoperated during this procedure, the robot could have still applied arbitrary forces while being compliant to active environments.

Complementary to a teleoperated robot as an active environment, the experiment in the health care setting provided additional insights. In this case, the EPRC-controlled robot was teleoperated and moved by a human directly, acting as the active environment. Similar to the space experiment, the EPRC induced an evasive motion of 40.85 cm at a maximal force of $F^{c} = 14$ N. Thus, considering the robot stiffness of $K^{t} = 600$ N/m and the resulting $\Delta p = 2.3$ cm, the EPRC increased the compliance by more than 1670%. This analysis confirmed that the EPRC-controlled robot can apply unrestricted forces in its environment, for instance, via teleoperation, while being plastically compliant at any time. The human motion initiated the plastic robot reaction, but as soon as the environment behaved

passively, the robot could directly apply forces in the respective directions. In contrast, comparable approaches restrict critically the force applicable by the robot, rely on environment models, or induce emergency stops.

The health care setting demonstrated that the EPRC and its SoA sensitivity in particular can place the robot in a subordinate role. This holds promise for accelerating the integration of assistance robots in health care facilities, because current norms and standards require the detection of humans. Thereby, the detection of humans via visual sensors is challenging given that potential occlusion of humans and sensor inaccuracies can occur. In contrast, the detection of the SoA as applied in the EPRC enables the detection of humans without visual sensing or accurate environment models.

SoA type 2 evaluation in space application

The space experiment on interaction with an articulated object (SoA type 2) confirmed that the robot was able to simultaneously follow a motion command and behave plastically in another DoF when an energy input from the environment was detected. The EPRC reaction proved to be particularly helpful in the case of delayed teleoperation because it adapted the robot's command to locally compensate for deviations from the required trajectory of the articulated object at the robot side. This local control was able to correct the deviation far earlier than the remote operator, who had to react to the delayed force feedback pushing the haptic device toward the trajectory. Although the astronaut supported the motion along the trajectory to some extent, the EPRC had an effect, compensating $p_{\%} = 54.7\%$ of the motion necessary to keep the robot reference pose on the required trajectory. The data revealed that the power threshold was set too high (because the force command to the robot was attenuated by the TDPA-HD, among others) such that the spatial spring had to be deflected more to reach higher force values and finally trigger the EPRC plasticity.

The laboratory experiment on SoA type 2 with the humanoid robot presented in the Supplementary Materials ("Experiments with Power-Based EPRC" section) confirmed that a power limit of $P_{\text{thr}} = 0.1$ J/s was applicable in a comparable task without risking erroneous activation of the EPRC. With this threshold, the EPRC could reduce the required motion by above $p_{\%} = 80\%$ in the delayed and undelayed cases.

The EPRC performance can be enhanced in future space missions, especially by less conservative power thresholds and slower and more continuous motion commands by the teleoperator, which reduce the force and power attenuation by the TDPA-HD. Despite the astronaut being a novice in teleoperation, they reported that they recognized the support in trajectory following, although the EPRC functionality was not explained to them in advance.

Limitations and future steps

The wide variety of abstract and realistic experiments with varying types of SoA presented in this work provided initial insights into the capabilities and performance of the newly introduced EPRC concept. However, limitations in the experimental design, as well as challenges of EPRC control, and important future research directions need to be acknowledged and are discussed in the following.

Although the EPRC robustness could be confirmed for the presented scenarios, a larger set of tasks needs to be investigated to evaluate the respective minimal force and power thresholds. In case of limited performance in specific situations, the use of force-torque sensors or disturbance observers or the consideration of mass models of grasped objects may help to optimize the EPRC. Regarding delay, a TDPA considering energy reflection (*45*) or proxy-based methods (*46*) that reduce force and power attenuation when compared with TDPA-HD may be more suitable in combination with the EPRC.

For instance, carrying of heavy objects requires particular attention in the EPRC because the load is potentially recognized as an active environment. If disabling the EPRC or increasing the force and power thresholds in the gravity direction is not desired, heavy objects need to be lifted up by the robot to avoid triggering the EPRC, whereas putting and releasing a load in the robotic hand would trigger a plastic reaction. In the first case, the robot deflects the coupling spring, whereas in the second case the load deflects the spring resembling an active behavior. Thereby, as discussed in the Supplementary Materials ("Experiments with Energy-Based EPRC" section), the energy-based EPRC promises higher robustness in gravity direction. However, it has to be noted that the power-based EPRC showed sufficient performance when operating the weight of the lever arm and pipe.

Another limitation of the experimental design was that all experiments were performed with DLR LWRs representing high-performance impedance-controlled robots. In future work, the applicability of the EPRC to low-cost manipulators, but also to more complex systems with variable spring actuators, should be investigated.

The potential of the EPRC goes far beyond the benefits presented in the experiments of this work. An additional analysis that is not in the scope of this work showed that the interaction of a manipulator attached to a flying system (*47*) with its environment can be enhanced in the case of wind disturbances through the EPRC. In this scenario, the EPRC can analyze the energy exchange at the contact with the environment to compensate for errors in the odometry of the flying system that would negatively affect an insertion task. This holds true similarly for odometry errors of wheeled or legged systems if the robot platform has to move while the platform's manipulator is in contact.

Besides these scenarios, future work should investigate whether the EPRC acting independently in each translational DoF of the robot base frame (as implemented here) can also be designed in the task frame. Furthermore, the possibility and benefits of treating the DoFs separately or conjointly in the EPRC should be studied. Moreover, upcoming space experiments seek the parallel control of the EPRC-controlled humanoid robot from a second input device to investigate more complex cooperation tasks with the ESA rover controlled from the ISS.

MATERIALS AND METHODS

Laboratory setup

The abstract laboratory experiments were performed with a DLR LWR (Fig. 8A). The EPRC was implemented on this robotic manipulator that was teleoperated via the lambda.7 haptic device from Force Dimension. The control software was running at a 1-kHz sampling rate, and the delay between the input device and robot was zero such that no control ensuring passivity despite communication delay was required. The stiffness of the virtual spatial spring coupling both systems was set to $K^{\text{LS,t}} = 400$ N/m in translations and $K^{\text{LS,r}} = 10$ Nm/rad in the rotations. The EPRC was enabled in all six Cartesian DoFs with the following parametrization: power limits $P^{\text{LS,t}}_{\text{thr}} = 0.1$ J/s and $P^{\text{LS,r}}_{\text{thr}} = 0.05$ J/s and force limits $F^{\text{LS,t}}_{\text{thr}} = 0.4$ N and $F^{\text{LS,r}}_{\text{thr}} = 0$ Nm.

Fig. 8. Experimental hardware. (**A**) The DLR LWR at the back was under EPRC control and could be controlled via the lambda.7 input device. (**B**) The sigma.7 haptic input device was applied in the experiments on the ISS and in the elderly care facility. (**C**) The wheelchair-based robot EDAN was equipped with an eight-DoF robotic manipulator and a DLR CLASH hand.

Space mission setup

The space experiment was part of the Surface Avatar project (*41*, *42*), a cooperation between DLR and ESA, and performed during the Axiom mission (*48*) in January 2024. The ESA IR hardware, as well as the ISS communication, was identical to the Analog-1 mission (*3*). However, a difference in this mission was that the ESA rover was now a part of a robotic team with the DLR humanoid robot, as well as DLR's quadruped Bert (not used in this work) to perform several experiments (*49*). The ESA rover (see left robot in Fig. 1A) was equipped with two DLR LWRs: one used as a pan-tilt unit for the monoscopic camera, the other for manipulation tasks. The latter robotic arm was controlled by an astronaut from the ISS in the SoA type 1 experiment through a space-qualified sigma.7 haptic device from Force Dimension. In addition, the astronaut on the ISS Columbus module (see Fig. 1B) was equipped with a graphical user interface providing mono visual feedback among other interfaces for supervised control. Via the button on the left-hand joystick, the astronaut enabled the coupling to the respective robot.

The KU-band communication to the ISS was built up via the Tracking and Data Relay Satellite System consisting of three clusters of satellites in geostationary orbit (35,700 km above Earth) such that the ISS and NASA's White Sands satellite complex in the United States was always visible. From White Sands, the communication passed via a transatlantic cable to Germany. The link had an average RTD of ~850 ms and was severely bandwidth-limited (4 Mbps in both directions). Stability despite delay was ensured via TDPA-HD. For more details on the ESA rover, the ISS communication, as well as the user interface on the ISS, the reader is referred to (*3*, *50*, *51*).

The humanoid robot RJ was equipped with 41 torque-controlled DoFs in the upper body, including 3 for the torso, 7 for each arm, and 12 for each hand. Its torque control interface facilitated the implementation of impedance-based reactive whole-body control (*52*, *53*), which was well suited for physical interactions with the environment. During the SoA type 2 experiment, the astronaut teleoperated the EPRC-controlled right arm of the humanoid robot with the sigma.7 device via TDPA-HD. In addition, the operator could directly command head and platform movements using the respective position and velocity control interfaces. The control software of all systems was running at a 1-kHz sampling rate. In contrast with the manipulator of the ESA rover, which was equipped with a force-torque sensor, a disturbance observer was used on the humanoid robot for force feedback as well as passivity observation and control in TDPA-HD.

The impedance controller of the ESA rover was parametrized with $K^{\mathrm{IR,t}} = 960$ N/m and $K^{\mathrm{IR,r}} = 38.4$ Nm/rad. The controller of the DLR humanoid robot was parametrized with $K^{\mathrm{RJ,t}} = 500$ N/m, $K^{\mathrm{RJ,r}} = 20$ Nm/rad, EPRC power limits $P^{\mathrm{RJ,t}}_{\mathrm{thr}} = 0.01$ J/s, and EPRC force limits $F^{\mathrm{RJ,t}}_{\mathrm{thr}} = 0.05$ N during the SoA type 1 experiment and with $K^{\mathrm{RJ,t}} = 500$ N/m, $K^{\mathrm{RJ,r}} = 50$ Nm/rad, $P^{\mathrm{RJ,t}}_{\mathrm{thr}} = 0.2$ J/s, and $F^{\mathrm{RJ,t}}_{\mathrm{thr}} = 0.4$ N during the SoA type 2 experiment. Note that in both scenarios the EPRC was only enabled in translations.

Tele–health care assistance setup

The experiments focusing on human-robot interaction took place in a Caritas elderly care facility in Garmisch-Partenkirchen, Germany. A sigma.7 (Fig. 8B) served as input device to teleoperate the mobile assistive robot DLR EDAN, depicted in Fig. 8C. EDAN (*54*) is an assistive robot for people with severe physical disability that can be controlled via a joystick or on the basis of measurements of muscular activity via electromyography devices (*55*). EDAN consists of a commercial powered wheelchair and a DLR LWR. The robotic manipulator is equipped with an additional pitch axis at the robot base extending the workspace such that reaching the ground with the end effector tool was feasible. A whole-body controller could move the wheelchair to further expand the workspace of the robotic arm in the horizontal plane in case the limits of its workspace were reached (*56*). The DLR CLASH hand mounted at the end effector of EDAN allowed for stable grasps through adaptive compliance (*57*). In total, including the 8-DoF robotic arm, the 7-DoF CLASH hand, and the 2 DoFs of the wheelchair, EDAN provided 17 DoFs.

The camera pair mounted on a pan-tilt unit provided a stereo video stream to the operator's head-mounted display (Fig. 8B) and was moved according to the head motion of the operator. Both the haptic device and EDAN were located at the elderly facility but

positioned in different rooms. The systems were connected via WiFi, resulting in an RTD below 100 ms between input device and robot. The control software of all systems was running at a 1-kHz sampling rate, and the stability despite communication delay was ensured via TDPA-HD. Analogous to the humanoid robot, a disturbance observer was applied for TDPA-HD because EDAN did not provide a force-torque sensor at the end effector. The impedance controller was tuned with $K^{\mathrm{ED,t}} = 600$ N/m and $K^{\mathrm{ED,r}} = 50$ Nm/rad, and the EPRC with $P_{\mathrm{thr}}^{\mathrm{ED,t}} = 0.01$ J/s, $P_{\mathrm{thr}}^{\mathrm{ED,r}} = 0.1$ J/s, $F_{\mathrm{thr}}^{\mathrm{ED,t}} = 0.05$ N, and $F_{\mathrm{thr}}^{\mathrm{ED,r}} = 0$ Nm.

Supplementary Materials

This PDF file includes:

Methods
Discussion
Figs. S1 to S19
Reference (*58*)

REFERENCES AND NOTES

1. Y. Michel, R. Rahal, C. Pacchierotti, P. R. Giordano, D. Lee, Bilateral teleoperation with adaptive impedance control for contact tasks. *IEEE Robot. Autom. Lett.* **6**, 5429–5436 (2021).
2. H. Su, J. Sandoval, M. Makhdoomi, G. Ferrigno, E. De Momi, Safety-enhanced human-robot interaction control of redundant robot for teleoperated minimally invasive surgery, in *2018 IEEE International Conference on Robotics and Automation (ICRA)* (IEEE, 2018), pp. 6611–6616.
3. M. Panzirsch, A. Pereira, H. Singh, B. Weber, E. Ferreira, A. Gherghescu, L. Hann, E. den Exter, F. van der Hulst, L. Gerdes, L. Cencetti, K. Wormnes, J. Grenouilleau, W. Carey, R. Balachandran, T. Hulin, C. Ott, D. Leidner, A. Albu-Schäffer, N. Y. Lii, T. Krüger, Exploring planet geology through force-feedback telemanipulation from orbit. *Sci. Robot.* **7**, eabl6307 (2022).
4. T. Tomić, S. Haddadin, Simultaneous estimation of aerodynamic and contact forces in flying robots: Applications to metric wind estimation and collision detection, in *2015 IEEE International Conference on Robotics and Automation (ICRA)* (IEEE, 2015), pp. 5290–5296.
5. J. Lee, S. Ryu, H. J. Kim, Stable flight of a flapping-wing micro air vehicle under wind disturbance. *IEEE Robot. Autom. Lett.* **5**, 5685–5692 (2020).
6. D. C. Fernández, G. A. Hollinger, Model predictive control for underwater robots in ocean waves. *IEEE Robot. Autom. Lett.* **2**, 88–95 (2017).
7. B. Whitsell, P. Artemiadis, Physical human–robot interaction (pHRI) in 6 DOF with asymmetric cooperation. *IEEE Access* **5**, 10834–10845 (2017).
8. R. K. Leskovar, J. Čamernik, T. Petrič, Leader–follower role allocation for physical collaboration in human dyads. *Appl. Sci.* **11**, 8928 (2021).
9. R. K. Leskovar, T. Petrič, Humans prefer collaborating with a robot who leads in a physical human-robot collaboration scenario, in *2021 20th International Conference on Advanced Robotics (ICAR)* (IEEE, 2021), pp. 935–941.
10. S. Satake, T. Tsumugiwa, R. Yokogawa, Effects of leader–follower information asymmetry on brain activity during human–human cooperative transport work, in *IECON 2022–48th Annual Conference of the IEEE Industrial Electronics Society* (IEEE, 2022), pp. 1–7.
11. A. Takai, F. Q., Y. Doibata, G. Lisi, T. Tsuchiya, K. Mojtahedi, T. Yoshioka, M. Kawato, J. Morimoto, M. Santello, Learning acquisition of consistent leader–follower relationships depends on implicit haptic interactions. *Sci. Rep.* **13**, 3476 (2023).
12. Y. Liu, R. Leib, D. W. Franklin, Follow the force: Haptic communication enhances coordination in physical human-robot interaction when humans are followers. *IEEE Robot. Autom. Lett.* **8**, 6459–6466 (2023).
13. T. Kobayashi, E. Dean-Leon, J. R. Guadarrama-Olvera, F. Bergner, G. Cheng, Whole-body multicontact haptic human–humanoid interaction based on leader–follower switching: A robot dance of the "box step." *Adv. Intell. Syst.* **4**, 2100038 (2022).
14. D. Whitney, Force feedback control of manipulator fine motions. *J. Dyn. Sys. Meas. Control* **99**, 91–97 (1977).
15. J. Salisbury, Active stiffness control of a manipulator in Cartesian coordinates, in *1980 19th IEEE Conference on Decision and Control Including the Symposium on Adaptive Processes* (IEEE, 1980), pp. 95–100.
16. D. J. Latornell, D. B. Cherchas, Force and motion control of a single flexible manipulator link. *Robot. Comput. Integr. Manuf.* **9**, 87–99 (1992).
17. N. Hogan, Impedance control: An approach to manipulation, in *1984 American Control Conference* (IEEE, 1984), pp. 304–313.
18. M. Schumacher, J. Wojtusch, P. Beckerle, O. Von Stryk, An introductory review of active compliant control. *Robot. Auton. Syst.* **119**, 185–200 (2019).
19. T. Bhattacharjee, G. Niemeyer, Antagonistic muscle based robot control for physical interactions, in *2015 IEEE International Conference on Robotics and Automation (ICRA)* (IEEE, 2015), pp. 298–303.
20. C. Yang, G. Ganesh, S. Haddadin, S. Parusel, A. Albu-Schaeffer, E. Burdet, Human-like adaptation of force and impedance in stable and unstable interactions. *IEEE Trans. Robot.* **27**, 918–930 (2011).
21. R. Bischoff, J. Kurth, G. Schreiber, R. Koeppe, A. Albu-Schäffer, A. Beyer, O. Eiberger, S. Haddadin, A. Stemmer, G. Grunwald, G. Hirzinger, The KUKA-DLR lightweight robot arm—A new reference platform for robotics research and manufacturing, in *ISR 2010 (41st International Symposium on Robotics) and ROBOTIK 2010 (6th German Conference on Robotics)* (VDE, 2010), pp. 1–8.
22. M. Iskandar, C. Ott, O. Eiberger, M. Keppler, A. Albu-Schäffer, A. Dietrich, Joint-level control of the DLR lightweight robot SARA, in *2020 IEEE/RSJ International Conference on Intelligent Robots and Systems (IROS)* (IEEE, 2020), pp. 8903–8910.
23. S. Haddadin, S. Parusel, L. Johannsmeier, S. Golz, S. Gabl, F. Walch, M. Sabaghian, C. Jähne, L. Hausperger, S. Haddadin, The Franka Emika robot: A reference platform for robotics research and education. *IEEE Robot. Autom. Mag.* **29**, 46–64 (2022).
24. B. Vanderborght, A. Albu-Schaeffer, A. Bicchi, E. Burdet, D. G. Caldwell, R. Carloni, M. Catalano, O. Eiberger, W. Friedl, G. Ganesh, M. Garabini, M. Grebenstein, G. Grioli, S. Haddadin, H. Hoppner, A. Jafari, M. Laffranchi, D. Lefeber, F. Petit, S. Stramigioli, N. Tsagarakis, M. Van Damme, R. Van Ham, L. C. Visser, S. Wolf, Variable impedance actuators: A review. *Robot. Auton. Syst.* **61**, 1601–1614 (2013).
25. S. Wolf, G. Grioli, O. Eiberger, W. Friedl, M. Grebenstein, H. Höppner, E. Burdet, D. G. Caldwell, R. Carloni, M. G. Catalano, D. Lefeber, S. Stramigioli, N. Tsagarakis, M. Van Damme, R. Van Ham, B. Vanderborght, L. C. Visser, A. Bicchi, A. Albu-Schäffer, Variable stiffness actuators: Review on design and components. *IEEE/ASME Trans. Mechatron.* **21**, 2418–2430 (2015).
26. S. Haddadin, A. Albu-Schäffer, O. Eiberger, G. Hirzinger, New insights concerning intrinsic joint elasticity for safety, in *2010 IEEE/RSJ International Conference on Intelligent Robots and Systems* (IEEE, 2010), pp. 2181–2187.
27. M. Panzirsch, M. Sierotowicz, R. Prakash, H. Singh, C. Ott, Deflection-domain passivity control of variable stiffnesses based on potential energy reference. *IEEE Robot. Autom. Lett.* **7**, 4440–4447 (2022).
28. M. Panzirsch, H. Singh, M. Sierotowicz, A. Dietrich, Extension of the deflection-domain passivity approach for variable stiffnesses to SO(3). *IEEE Robot. Autom. Lett.* **9**, 2925–2932 (2024).
29. A. De Luca, A. Albu-Schaffer, S. Haddadin, Gerd Hirzinger, Collision detection and safe reaction with the DLR-iii lightweight manipulator arm, in *2006 IEEE/RSJ International Conference on Intelligent Robots and Systems* (IEEE, 2006), pp. 1623–1630.
30. M. Iskandar, O. Eiberger, A. Albu-Schäffer, A. De Luca, A. Dietrich, Collision detection, identification, and localization on the DLR SARA robot with sensing redundancy, in *2021 IEEE International Conference on Robotics and Automation (ICRA)* (IEEE, 2021), pp. 3111–3117.
31. A. De Luca, F. Flacco, Integrated control for pHRI: Collision avoidance, detection, reaction and collaboration, in *2012 4th IEEE RAS & EMBS International Conference on Biomedical Robotics and Biomechatronics (BioRob)* (IEEE, 2012), pp. 288–295.
32. S. Haddadin, A. Albu-Schaffer, A. De Luca, G. Hirzinger, Collision detection and reaction: A contribution to safe physical human-robot interaction, in *2008 IEEE/RSJ International Conference on Intelligent Robots and Systems* (IEEE, 2008), pp. 3356–3363.
33. M. Kyrarini, F. Lygerakis, A. Rajavenkatanarayanan, C. Sevastopoulos, H. R. Nambiappan, K. K. Chaitanya, A. R. Babu, J. Mathew, F. Makedon, A survey of robots in healthcare. *Technologies* **9**, 8 (2021).
34. J. Vogel, D. Leidner, A. Hagengruber, M. Panzirsch, B. Bauml, M. Denninger, U. Hillenbrand, L. Suchenwirth, P. Schmaus, M. Sewtz, A. S. Bauer, T. Hulin, M. Iskandar, G. Quere, A. Albu-Schaffer, A. Dietrich, An ecosystem for heterogeneous robotic assistants in caregiving: Core functionalities and use cases. *IEEE Robot. Auton. Mag.* **28**, 12–28 (2020).
35. J. Mišeikis, P. Caroni, P. Duchamp, A. Gasser, R. Marko, N. Mišeikienė, F. Zwilling, C. De Castelbajac, L. Eicher, M. Früh, H. Früh, Lio-a personal robot assistant for human-robot interaction and care applications. *IEEE Robot. Autom. Lett.* **5**, 5339–5346 (2020).
36. S. Dafarra, U. Pattacini, G. Romualdi, L. Rapetti, R. Grieco, K. Darvish, G. Milani, E. Valli, I. Sorrentino, P. M. Viceconte, A. Scalzo, S. Traversaro, C. Sartore, M. Elobaid, N. Guedelha, C. Herron, A. Leonessa, F. Draicchio, G. Metta, M. Maggiali, D. Pucci, iCub3 avatar system: Enabling remote fully immersive embodiment of humanoid robots. *Sci. Robot.* **9**, eadh3834 (2024).
37. J. Arents, V. Abolins, J. Judvaitis, O. Vismanis, A. Oraby, K. Ozols, Human–robot collaboration trends and safety aspects: A systematic review. *J. Sens. Actuator Netw.* **10**, 48 (2021).
38. M. Valori, A. Scibilia, I. Fassi, J. Saenz, R. Behrens, S. Herbster, C. Bidard, E. Lucet, A. Magisson, L. Schaake, J. Bessler, G. B. Prange-Lasonder, M. Kühnrich, A. B. Lassen,

K. Nielsen, Validating safety in human–robot collaboration: Standards and new perspectives. *Robotics* **10**, 65 (2021).
39. R.-J. Halme, M. Lanz, J. Kämäräinen, R. Pieters, J. Latokartano, A. Hietanen, Review of vision-based safety systems for human-robot collaboration. *Proc. CIRP* **72**, 111–116 (2018).
40. S. Haddadin, Method and device for open-loop/closed-loop control of a robot manipulator, US Patent US10464210B2 (2019).
41. N. Y. Lii, P. Schmaus, D. Leidner, T. Krueger, J. Grenouilleau, A. Pereira, A. Giuliano, A. S. Bauer, A. Köpken, F. Lay, M. Sewtz, N. Bechtel, S. B. Gomez, M. Denninger, W. Friedl, J. Butterfass, E. Ferreira, A. Gherghescu, T. Chupin, Emiel den Exter, L. Gerdes, M. Panzirsch, H. Singh, R. Balachandran, T. Hulin, T. Gumpert, A. Schmidt, D. Seidel, M. Hermann, M. Maier, R. Burger, F. Schmidt, B. M. Weber, R. Bayer, B. Pleintinger, R. Holderried, P. Pavelski, A. Wedler, Stefan von Dombrowski, H. Maurer, M. Görner, T. Wüsthoff, S. Bertone, T. Müller, G. Söllner, C. Ehrhardt, L. Brunetti, L. Holl, M. Bévan, R. Muehlbauer, G. Visentin, A. Albu-Schäeffer, Introduction to surface avatar: The first heterogeneous robotic team to be commanded with scalable autonomy from the ISS, in *Proceedings of the International Astronautical Congress, IAC* (International Astronautical Federation, 2022).
42. P. Schmaus, A. Bauer, N. Bechtel, M. Denninger, A. Köpken, F. Lay, F. Schmidt, M. Sewtz, T. Krüger, D. Leidner, A. Pereira, N. Y. Lii, Extending the knowledge driven approach for scalable autonomy teleoperation of a robotic avatar, in *2023 IEEE Aerospace Conference* (IEEE, 2023), pp. 1–10.
43. R. Roll, J. C. Gilhodes, J. P. Roll, K. Popov, O. Charade, V. Gurfinkel, Proprioceptive information processing in weightlessness. *Exp. Brain Res.* **122**, 393–402 (1998).
44. U. Proske, B. M. Weber, Proprioceptive disturbances in weightlessness revisited. *npj Microgravity* **9**, 64 (2023).
45. M. Panzirsch, J.-H. Ryu, M. Ferre, Reducing the conservatism of the time domain passivity approach through consideration of energy reflection in delayed coupled network systems. *Mechatronics* **58**, 58–69 (2019).
46. H. Singh, M. Panzirsch, A. Coelho, C. Ott, Proxy-based approach for position synchronization of delayed robot coupling without sacrificing performance. *IEEE Robot. Autom. Lett.* **5**, 6599–6606 (2020).
47. Y. S. Sarkisov, M. J. Kim, D. Bicego, D. Tsetserukou, C. Ott, A. Franchi, K. Kondak, Development of sam: Cable-suspended aerial manipulator, in *2019 International Conference on Robotics and Automation (ICRA)* (IEEE, 2019), pp. 5323–5329.
48. N. Y. Lii, T. Krueger, P. Schmaus, D. Leidner, N. Batti, A. S. Bauer, J. Butterfass, W.Friedl, T. Gumpert, A. Koepken F. S. Lay, X Luo, R. Luz, A.N. Manaparampil, L. Mayershofer, M. Panzirsch, P. Pavelski, A. Raffin, M. Sewtz, A. Schmidt, F. Schmidt, D. Seidl, H. Singh, C. Ehrhardt, M. Beven, L. Brunetti, L. Holl, R. Muelbauer G. Visentin, and A. Albu-Schaeffer, Everything is awesome if you are part of a (robotic) team: Preliminary insights from the first ISS-to-surface multi-robot collaboration with scalable autonomy teleoperation, in *75rd International Astronautical Congress (IAC)* (International Astronautical Federation, 2024).
49. P. Schmaus, P. Schmaus, This person is not on Research Gate, or hasn't claimed this research yet., D. Leidner, T. Krueger, J. Grenouilleau, A. Pereira, A. S. Bauer, N. Bechtel, S. B. Gomez, A. Köpken, F. Lay, M. Sewtz, N. Batti, E. Ferreira, Emiel den Exter, R. Bayer, B. Pleintinger, R. Holderried, P. Pavelski, N. Y. Lii, On realizing multi-robot command through extending the knowledge driven teleoperation approach, in *Proceedings of the International Astronautical Congress, IAC* (International Astronautical Federation, 2022).
50. T. Krueger, E. Ferreira, A. Gherghescu, L. Hann, E. den Exter, Frank PJ van der Hulst, Levin Gerdes, Aaron Pereira, Harsimran Singh, Michael Panzirsch, T. Hulin, R. Balachandran, B. M. Weber, N. Y. Lii, Designing and testing a robotic avatar for space-to-ground teleoperation: The developers' insights, in *71st International Astronautical Congress, IAC 2020* (International Astronautical Federation, 2020).
51. K. Wormnes, W. Carey, T. Krueger, L. Cencetti, E. den Exter, S. Ennis, E. Ferreira, A. Fortunato, L. Gerdes, L. Hann, C. Lombardi, E. Luzzi, S. Martin, M. Massironi, S. Payler, A. Pereira, A. P. Rossi, R. Pozzobon, F. Sauro, P. Schoonejans, F. van der Hulst, J. Grenouilleau, ANALOG-1 ISS—The first part of an analogue mission to guide ESA's robotic moon exploration efforts. *Open Astron.* **31**, 5–14 (2022).
52. A. Dietrich, T. Wimbock, A. Albu-Schaffer, G. Hirzinger, Reactive whole-body control: Dynamic mobile manipulation using a large number of actuated degrees of freedom. *IEEE Robot. Autom. Mag.* **19**, 20–33 (2012).
53. X. Wu, C. Ott, A. Albu-Schäffer, A. Dietrich, Passive decoupled multitask controller for redundant robots. *IEEE Trans. Control Syst. Technol.* **31**, 1–16 (2023).
54. J. Vogel, A. Hagengruber, M. Iskandar, G. Quere, U. Leipscher, S. Bustamante, A. Dietrich, H. Höppner, D. Leidner, A. Albu-Schäffer, EDAN: An EMG-controlled daily assistant to help people with physical disabilities, in *2020 IEEE/RSJ International Conference on Intelligent Robots and Systems (IROS)* (IEEE, 2020), pp. 4183–4190.
55. A. Hagengruber, J. Vogel, Functional tasks performed by people with severe muscular atrophy using an semg controlled robotic manipulator, in *2018 40th Annual International Conference of the IEEE Engineering in Medicine and Biology Society (EMBC)* (IEEE, 2018), pp. 1713–1718.
56. M. Iskandar, G. Quere, A. Hagengruber, A. Dietrich, J. Vogel, Employing whole-body control in assistive robotics, in *2019 IEEE/RSJ International Conference on Intelligent Robots and Systems (IROS)* (IEEE, 2019), pp. 5643–5650.
57. W. Friedl, H. Höppner, F. Schmidt, M. A. Roa, M. Grebenstein, CLASH: Compliant low cost antagonistic servo hands, in *2018 IEEE/RSJ International Conference on Intelligent Robots and Systems (IROS)* (IEEE, 2018), pp. 6469–6476.
58. R. M. Murray, Z. Li, S. S. Sastry, *A Mathematical Introduction to Robotic Manipulation* (CRC Press, 1994).

Acknowledgments: We thank our colleagues at the German Space Operation Center (GSOC) for their support on network communication and ISS operation, those at the European Astronaut Centre (EAC) for the astronaut training in the Surface Avatar experiment, and G. Visentin and J. Grenouilleau of ESA for enabling the cooperation with DLR. **Funding:** This work was partly supported by the Bavarian Ministry of Economic Affairs, Regional Development and Energy, within the project "SMiLE2gether" (LABAY102) and partially supported by the DLR-ESA Joint-Lab Agreement. **Author contributions:** The author list is sorted in alphabetical order from R.B. to F.S. M.P. (control lead) and H.S. developed and implemented the elasto-plastic controller and performed the laboratory experiments.X.W. worked on the hand and whole-body control of DLR RJ. M.I., A.H., G.Q., S.B.-G., and J.V. managed DLR EDAN planning and infrastructure. A.H., J.V., and M.P. performed the elderly care experiments. R.L. was responsible for the teleoperation of the ESA Interact Rover. N.B. developed DLR RJ high-level software and infrastructure. A.S.B. was responsible for DLR RJ and developing high-level software and infrastructure. A.K. developed DLR RJ high-level software and infrastructure. F.S.L. developed DLR RJ high-level software, space-to-ground communication link, and on-board ISS software infrastructure. X.L. worked on perception for DLR RJ and space-to-ground communication link. A.N.M. worked on space-to-ground communication link and on-board ISS software. L.M. worked on knowledge-driven user interfaces (UIs). P.S. led the development of the knowledge-driven UI. E.d.E. worked on knowledge-driven UI element design. For the hardware and software infrastructure: J.B. was responsible for the DLR RJ hand mechatronics. W.F. was responsible for the DLR RJ mechatronics systems and the DLR CLASH hand. T.G. was responsible for the DLR RJ mechatronics systems. R.B. and F.S. developed the software infrastructure on ground for DLR RJ. P.P. contributed experimental environment design and development. For the administration: N.Y.L., principal investigator (PI) of the space project Surface Avatar, supported with space experiments. J.V. was the PI of the health care assistance robotics project SMiLE. T.K. was the lead of the ESA contribution and supported with space experiments. D.L. and A.A.-S. managed the DLR contribution. P.S., D.L., and T.K. were coinvestigators of the space project Surface Avatar. For the analysis: M.P. and H.S. analyzed the metrics in the objective data. For the manuscript: M.P., H.S., X.W., M.I., J.V., and N.Y.L. discussed the results, and all other authors commented. M.P. prepared the manuscript. **Data and materials availability:** The data for this study have been deposited in the Zenodo database with DOI 10.5281/zenodo.14749400. All other data needed to evaluate the conclusions in the paper are present in the paper or the Supplementary Materials.

Submitted 30 April 2024
Accepted 29 January 2025
Published 26 February 2025
10.1126/scirobotics.adq1703

Science Robotics

Virtual elasto-plastic robot compliance to active environments

Michael Panzirsch, Harsimran Singh, Xuwei Wu, Maged Iskandar, Anne Koepken, Rute Luz, Nesrine Batti, Florian S. Lay, Ajithkumar Narayanan Manaparampil, Luisa Mayershofer, Xiaozhou Luo, Robert Burger, Samuel Bustamante-Gomez, Jörg Butterfass, Emiel den Exter, Werner Friedl, Thomas Gumpert, Pedro Pavelski, Gabriel Quere, Florian Schmidt, Alin Albu-Schaeffer, Adrian S. Bauer, Daniel Leidner, Peter Schmaus, Annette Hagengruber, Thomas Krueger, Jörn Vogel, and Neal Y. Lii

Sci. Robot. **10** (99), eadq1703. DOI: 10.1126/scirobotics.adq1703

Science Robotics (ISSN 2470-9476) is published by the American Association for the Advancement of Science. 1200 New York Avenue NW, Washington, DC 20005. The title *Science Robotics* is a registered trademark of AAAS.